Composite Structures 307 (2023) 116645

Contents lists available at ScienceDirect

Composite Structures

journal homepage: www.elsevier.com/locate/compstruct

A numerical–analytical study to determine a suitable distribution of plies in sandwich structures subjected to high-velocity impact

L. Alonso [a], A. Solis [b,*], S.K. García-Castillo [c]

[a] Department of Chemical Technology, Energy and Mechanics, Rey Juan Carlos University, C/Tulipán s.n. 28933, Spain
[b] Department of Mechanical Engineering and Industrial Design, University of Cádiz, Avda. de la Universidad de Cádiz 10, 11519, Puerto Real (Cádiz), Spain
[c] Department of Continuum Mechanics and Structural Analysis, University Carlos III of Madrid, Avda de la Universidad 30, 28911 Leganés, Madrid, Spain

ARTICLE INFO

Keywords:
Energy-absorption
Foam
Analytical modelling
Numerical modelling
High-velocity impact

ABSTRACT

This work presents a study that was undertaken to find the configuration that corresponds to the highest ballistic limit for composite sandwich structures made of glass fibre-reinforced polymer (GFRP) sandwich skins and a crushable foam. To this end, a new three-dimensional finite element (FE) model was implemented. The model accounts for the constitutive response of the GFRP sandwich skins and the crushable foam by means of two subroutines. A previously developed analytical model was used to support and complete the results of the FE model. Experimental data were also used to validate both models in the vicinity of the ballistic limit for the neutral configuration (same number of plies on the front and rear face skins). Thus, the most appropriate configuration to improve the ballistic limit for a structure with the same material (same number of plies) was obtained by testing different distributions of laminae. The ballistic limit was then estimated for all the possible configurations and the energy-absorption mechanisms were analysed to reveal new insights into the behaviour of these structures when the neutral configuration is varied. In addition, the damaged areas of the specimens were compared between the experiments and the model. As a result, the most suitable configuration turned out to be associated with thicker rear face skins, which produce higher ballistic limits. The largest fraction of the energy was absorbed by the out-of-plane mechanisms, this behaviour being maintained in all the configurations. Experimental observations established that the damaged area of the front face skin was smaller than the damage produced in the rear face skin and that bending effects were notable in the latter. The affected areas were proved to have a round shape, presenting the largest size in the vicinity of the ballistic limit.

1. Introduction

It is well established that composite structures provide good resistance-weight and stiffness-weight ratios compared to traditional materials such as steel, titanium or aluminium. These ratios enable the amount of material needed and hence the costs to be significantly reduced [1,2]. One of the most paradigmatic typologies is composite laminate, which allows the possibility of varying the stacking sequence or ply orientation to strengthen rigidity only in the direction in which loads are applied, lightening the weight. Within this context, the existence of models based on continuum mechanics [3] that can predict free-edge interlaminar stresses is highly desirable, given the structural weakening that free-edge effects may cause [4]. Moreover, the presence of notches and holes in the specimen that are inherent to the manufacturing process may also introduce intensification stress factors that are associated with failure mechanisms such as delamination [5,6], combined with fibre microbuckling in compression or fibre debonding in traction states [7–9]. Delamination may even be promoted depending on ply orientation in compression or flexural states [10].

Woven composite laminates are used in aerospace, maritime and military applications in which high-velocity impacts impose compression and shear loads [11–14]. Natural fibre-reinforced polymer composites [15] are also widely used in bulletproof vests and ballistic applications. In this regard, sandwich structures with a foam core have been thoroughly studied. [16] found fibre breakage in the front and rear faces, with delamination of the inner plies and shear failure in the core when sandwich skins with different thicknesses are impacted by low-velocity projectiles. [17] showed the importance of the foam core, which allows the damaged area of the sandwich skins to be reduced, even when the residual velocity and the ballistic limit are quite similar to those corresponding to a pair of spaced sandwich skins

* Corresponding author.
E-mail addresses: luis.alonso.sanjose@urjc.es (L. Alonso), alberto.solis@uca.es (A. Solis).

https://doi.org/10.1016/j.compstruct.2022.116645
Received 7 March 2022; Received in revised form 24 November 2022; Accepted 27 December 2022
Available online 2 January 2023

List of acronyms

CFRP	Carbon fibre reinforced polymer
DOFs	Degrees of freedom
FE	Finite element
FEM	Finite element method
GFRP	Glass fibre reinforced polymer
I-P (O-O-P)	In-plane (out-of-plane)
NDE	Non-destructive evaluation
PVC	Polyvinyl chloride
VUMAT	Vectorised user material
VUSDFLD	Vectorised user subroutine to redefine field variables

without a material core. The shock front of the compression wave in the foam core produces higher piercing forces under impact loading, due to enhanced strength provided by the foam core [18]. Sandwich structures with a metal foam core are also used, given their capacity to significantly dissipate the kinetic energy of the projectile and restrain the formation of high stress regions [19]. Curvature of the panels changes the energy absorption rates: doubly curved sandwich panels have increased high-velocity impact resistance [20].

A ballistic equation was developed in order to describe the behaviour of composite structures with carbon fibre reinforced plastic sandwich skins with an aluminium honeycomb core under a hyper-velocity impact regime [21]. Various sandwich skin thicknesses were considered to review the velocity limits at the transition from the ballistic to the shatter regime at the onset of projectile fragmentation, and from the shatter to the hyper-velocity regime. An experimental and numerical study [22] showed optimal facesheet-thickness-to-core-thickness ratios in GFRP sandwich structures, seeking to identify the performance with the highest energy absorbed by the core, reducing overall deflection of the structure. In this case, the sandwich structures were subjected to underwater impulsive loads, since it has been established that underwater environments produce a significant difference in response compared to air-backed structures. In general terms, thicker and lower-density cores provide superior blast mitigation and failure resistance [23].

Sandwich panels consisting of titanium facesheets and an aluminium honeycomb core mainly absorb energy in the rear facesheet in symmetrical configurations [24]. Additionally, it has been found that carbon fibre-reinforced polymer (CFRP) with thinner sandwich skins bonded by an adhesive to thicker honeycomb Kevlar cores are more susceptible to damage if subjected to thermal fatigue [25]. It has been established that increasing facesheet thickness and reducing honeycomb cell size increases perforation resistance when the areal density of the sandwich structure exceeds a certain value [26]. For all these reasons, composite structure behaviour is more difficult to characterise than that of traditional materials when there are fatigue and fracture effects. Thus, the ability to inspect and characterise sandwich structures using non-destructive evaluation (NDE) methods [27] seems fundamental. NDE methods are even used to inspect sandwich structures with a balsa core [28] that can be used to build civil constructions in areas with severe climate conditions, given that they are capable of withstanding impacts from small projectiles such as secondary debris from blast, hurricanes, and tornados and foreign object debris from roads and runways.

Another possibility is provided by analytical models [29–31] that allow global magnitudes such as ballistic limits or residual velocities to be obtained with lower computational costs. This mathematical modelling technique assumes a series of stages that take into account data from previous stages in order to initialise later stages. For instance, [32] used the plastic work dissipated in deformation and fracture at each stage as an approximation from the solution of the previous stage. Shear forces are transmitted in the bond between facesheets and honeycomb core that are subjected to the impact of blunt and spherical projectiles. In these approximations, wave theory [33] is used as a way to calculate the effects of the impact through the material, which naturally introduces the failure mechanisms formulation [34], and it can be also applied to describe low-velocity regimes [35] or high-velocity impact in sandwich panels made of composite sandwich skins with dense cores [36].

As shown, a complete description of sandwich structures subjected to different impact velocities calls for a combination of analytical and numerical approaches that need to be endorsed by experimental observations. In this paper, we present a sensitivity study to determine the most suitable distribution of laminae in order to improve the ballistic limit with a given number of plies. The study is carried out numerically by using a continuum damage model implemented by means of a FE model based on two subroutines. One of them is associated with different failure criteria for the GFRP sandwich skins [37]. The other subroutine, specifically designed for this work, implements the constitutive law of the crushable foam core. The two subroutines are executed together. The numerical results are supported by the solution obtained from an analytical model previously developed and validated by the authors [38]. Both sets of results are carefully compared and discussed. Lastly, the numerically estimated damaged area is compared with the experimentally measured area affected by the projectile in specimens subjected to high-velocity impacts.

2. Finite element modelling

In this section, an explanation of the FE model to describe high-velocity impact in sandwich structures is presented. Two damage models are developed with the aid of two user-written subroutines in an explicit finite element method (FEM) framework (Abaqus/Explicit). For the first, a previously developed continuum damage mechanics model with different failure criteria is used by means of a vectorised user material (VUMAT) subroutine for the glass-fibre sandwich skins [39]. Note that the sandwich skins consist of perpendicularly interlaced fibres that are parallel with the laminate border, so the stacking sequence of the woven alignment form is always $[0/90]_{ns}$. For the other model, a crushable foam model is implemented adding a user-defined failure criterion. In the first two subsections, the constitutive model for the composite sandwich skins and foam core are described, taking into account failure mechanisms related to those considered in the theoretical model, which will be summarised in the next section and are fully explained in [38]. In the third subsection, the discretisation type of the elements is described.

2.1. Constitutive model for the sandwich skins

Based on the experimental evidence, the constitutive response of the glass-fibre sandwich skins can be assumed to be linear-elastic up to the onset of damage, which means that the sandwich starts deteriorating, being orthotropic. This being so, it is a reasonable assumption that such a constitutive material law is progressively affected by the projectile. The damage by different mechanisms is taken into account through six scalar damage variables that affect the diagonal terms. Since damage variables evolve differently, the material can separate merely from being orthotropic. However, non-diagonal terms remain unaffected, which could be a limitation if damage behaves asymmetrically. Nevertheless, this type of constitutive law is widely used [40–43]. Furthermore specimens analysed in this work, as shown in latter sections, present a circular damaged surface after impact reinforcing the

hypothesis of symmetric damage. The constitutive behaviour is then formulated in Mandel's notation as:

$$\begin{bmatrix}\varepsilon_{11}\\ \varepsilon_{22}\\ \varepsilon_{33}\\ \gamma_{12}\\ \gamma_{23}\\ \gamma_{13}\end{bmatrix}=\begin{bmatrix}\frac{1}{E_{11}(1-d_1)} & -\frac{\nu_{21}}{E_{22}} & -\frac{\nu_{31}}{E_{33}} & 0 & 0 & 0\\ -\frac{\nu_{12}}{E_{11}} & \frac{1}{E_{22}(1-d_2)} & -\frac{\nu_{32}}{E_{33}} & 0 & 0 & 0\\ -\frac{\nu_{13}}{E_{11}} & -\frac{\nu_{23}}{E_{22}} & \frac{1}{E_{33}(1-d_3)} & 0 & 0 & 0\\ 0 & 0 & 0 & \frac{1}{G_{12}(1-d_4)} & 0 & 0\\ 0 & 0 & 0 & 0 & \frac{1}{G_{23}(1-d_5)} & 0\\ 0 & 0 & 0 & 0 & 0 & \frac{1}{G_{13}(1-d_6)}\end{bmatrix}\begin{bmatrix}\sigma_{11}\\ \sigma_{22}\\ \sigma_{33}\\ \sigma_{12}\\ \sigma_{23}\\ \sigma_{13}\end{bmatrix} \tag{1}$$

where ε_{ii} and γ_{ij} (with $i,j=1,2,3$) are the components of the strain tensor, σ_{ij} are the components of the stress tensor; E_{ii}, ν_{ij} and G_{ij} are the Young's moduli, Poisson's coefficients and shear moduli, respectively, and d_i are damage parameters associated with different failure mechanisms. Once the onset of damage in a particular direction is reached, a linear decay controlled by the fracture toughness is produced along that direction. As will be described in the theoretical model, failure criteria can be divided into in-plane and out-of-plane types. Some hypotheses are assumed theoretically to simplify the model and thus some energy-absorption mechanisms are neglected depending on the behaviour of the sandwich skins due to the boundary conditions, thickness, etc. Nevertheless, the failure criteria presented in the FE model account for all the possible energy-absorption mechanisms. In-plane tensile and compression fibre failure associated with fibre failure and elastic deformation of fibres [37] are triggered once the following criteria are met [44]:

$$\left(\frac{\sigma_{11}}{X_{11i}}\right)^2+\left(\frac{\sigma_{12}}{S_{12}}\right)^2+\left(\frac{\sigma_{13}}{S_{13}}\right)^2=1 \tag{2}$$

$$\left(\frac{\sigma_{22}}{X_{22i}}\right)^2+\left(\frac{\sigma_{12}}{S_{12}}\right)^2+\left(\frac{\sigma_{13}}{S_{13}}\right)^2=1, \tag{3}$$

where X_{llr} are the normal failure stresses, S_{lk} are the shear failure stresses associated with $l,k=1,2,3$, and $r=(t,c)$ accounts for tension and compression. X_{lkr} and S_{lk} were calculated according to Standards [45,46] and can be found respectively in [31,37]. According to [47], failure by matrix cracking is caused by the in-plane shear tension when the following relation is reached:

$$\left(\frac{\sigma_{12}}{S_{12s}}\right)^2=1, \tag{4}$$

where S_{12s} is the shear failure stress associated with matrix cracking [40]. S_{12s} is calculated according to Standard [46] and can be found in [31]. The through-thickness matrix and fibre failure criterion is associated with shear plugging and assumed to be caused by the out-of-plane shear stress components, leading to:

$$\left(\frac{\sigma_{13}}{S_{13s}}\right)^2+\left(\frac{\sigma_{23}}{S_{23s}}\right)^2=1, \tag{5}$$

where S_{13s} and S_{23s} are the shear failure stresses associated with matrix breakage in the through-the-thickness direction. S_{13s} and S_{23s} were calculated according to Standard [46] and can be found in [31]. Finally, the crush failure criterion is associated with compression along the thickness direction of the sandwich skins and is defined as:

$$\left(\frac{\sigma_{33}}{X_{33}}\right)^2=1, \tag{6}$$

where X_{33} is the normal failure stress in the through-the-thickness direction. X_{33} is calculated according to Standard [48] and can be found in [49]. The interlaminar damage model used in the finite element analysis is based on the classical cohesive zone method by means of a traction-separation law [50]. Further details about the formulation of this model can be found in [37].

2.2. Constitutive model for the foam

The constitutive response of the polyvinyl chloride (PVC) foam was experimentally obtained in the literature [51] by means of several uniaxial compression tests which provide the typical compression stress-strain curve for crushable foams. The curve obtained can be modelled by means of three stages. In the first stage, the foam exhibits a linear-elastic behaviour up to a certain level of stress, named the yield stress, where the strain can be increased while the stress remains constant. This is well-known as the plateau region. The Young's modulus and the initial Poisson's coefficient are E = 87 MPa and $\nu = 0.3$ respectively. Following this, the cells of the foam start to collapse, leading to a densification process where the stress increases with the strain. The remaining properties for the plateau and densification region can be found in [38]. To reproduce this behaviour, a crushable foam model with isotropic hardening was chosen. This model is governed by the equivalent plastic strain and assumes a similar behaviour in tension and compression. The data from uniaxial tests performed by [51] is sufficient to describe the evolution of the yield surface. Some unavailable parameters such as the ratio between the initial yield stress in uniaxial compression and in hydrostatic compression (k = 0.95), and the plastic Poisson's coefficient ($\nu_p = 0.0004$) had to be estimated according to [52]. Nevertheless, this model does not incorporate a criterion for element deletion during the impact process. This is the reason why an additional vectorised user subroutine to redefine field variables at a material point (VUSDFLD) was used to implement the same criteria as those considered in the theoretical model described below for the foam region. The two criteria are compression and shear plugging, which are respectively:

$$\left(\frac{\sigma_{33}}{X_{33f}}\right)^2=1 \tag{7}$$

$$\left(\frac{\sigma_{23}}{S_{23f}}\right)^2+\left(\frac{\sigma_{13}}{S_{13f}}\right)^2=1, \tag{8}$$

where X_{33f} is the normal failure stress of the foam in the through-the-thickness direction and S_{13f} and S_{23f} are the shear failure stresses of the foam. Once one of these criteria is met, the element is deleted.

2.3. Finite element implementation

The model is formulated for dynamic analysis and explicit integration and is coded as an Abaqus/Explicit VUMAT user-subroutine. Three-dimensional Lagrangian elements were used to carry out the simulations. The dimensions of the sandwich plates were (160 × 160 mm^2). This size ensured that the damage would not reach the edge of the specimen and therefore boundary conditions would not influence the damage. The skins of the sandwich used in this study were made from E-glass/polyester woven laminates. The core of the sandwich was a PVC foam with a density of 100 kg/m^3, and the skins were 1980 kg/m^3. The foam core was 30 mm thick as in the experimental specimens (see Fig. 1(a)). Each ply was 0.6 mm thick and a total of ten plies were used in all the configurations studied, as described in the results section. Ten plies were also used in the experimental tests, five in the front skin and five in the rear skin. For a better understanding of the simulated conformations in the FE model, Fig. 1(b) illustrates two (1-9 and 6-4) of the configurations simulated as an example. The first number is the number of plies in the front sandwich skin (0.6 mm each) and the second number denotes the plies in the back sandwich skin. Configurations ranging from 1-9 to 9-1 were studied, 5-5 being the configuration corresponding to the available experimental data. Due to the perpendicular alignment of the fibres, the constitutive response of the E-glass polyester laminates was taken to be orthotropic, with nine independent constants given by [37]. A VUMAT subroutine developed by [37] was used to account for the continuum damage model.

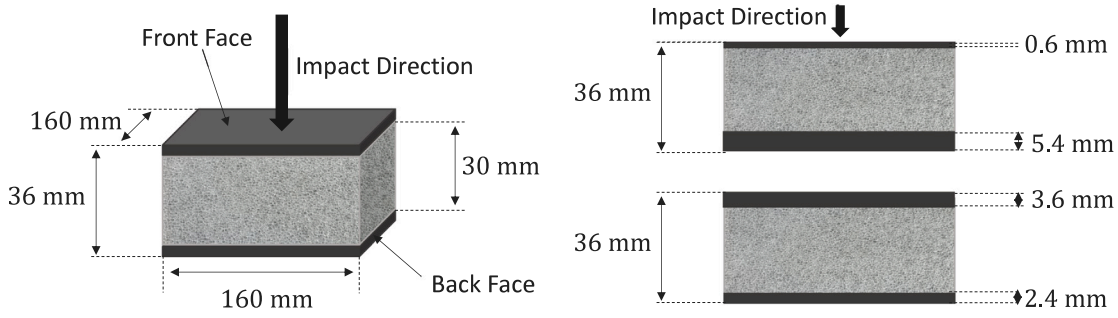

(a) Overall sandwich dimensions (b) Reference configurations. 1-9 (top). 6-4 (bottom)

Fig. 1. Sandwich structure and reference configurations.

The model is composed of 502425 C3D8R hexahedral elements for the plies (Abaqus notation). Since C3D8R are reduced integration elements whose stiffness matrix is calculated through a single integration point, so three degrees of freedom (DOFs) are available per element. 111650 COH3D8 hexahedral elements were used in the model as the cohesive elements to simulate the joints. Since COH3D8 are complete integration elements with four points of integration, twelve DOFs are available per element. The model is composed of 627536 nodes. At each node, three DOFs related to the three spatial displacements are available. The constitutive behaviour of the cohesive elements is defined by means of a traction-separation law where the stress vector is calculated as the elasticity matrix multiplied by the strains, defined as the separations divided by the initial thickness of the cohesive element [52]. The onset of damage is reached when a function involving the nominal stress ratios is equal to one and from that point, damage evolves according to the Benzeggagh-Kenane fracture criterion [53]. The equations and material properties needed to define the constitutive behaviour of this interlaminar damage model are collected in [37].

In addition, among the methods to avoid the problem of growth of cracks through preferred paths attached to mapped meshes [54–56], an unstructured mesh as shown in Fig. 2 was used. A convergence study varying the areal mesh density was carried out in a previous study [37] for the same geometry, obtaining differences of less than 1% from the results with this mesh. This analysis ensures the independence of the results when using a finer mesh in the impact region with elements of $0.5 \times 0.5 \times 0.3$ mm^3 and increasing the element size outwards from the impact location. The longitudinal element density ensures that the criterion established by [52] is met, with elements 0.3 mm thick within the plies and 2 mm thick within the foam. This distribution ensures a good degree of accuracy in the centre where the impact takes place, and at the same time the gradient proposed along the free mesh enables the problem described below to be avoided, reducing the number of elements and thus being computationally more efficient. This division can be seen in Fig. 2. Fig. 2(a) shows the whole sandwich panel meshed while Fig. 2(b) shows a detail of the more finely meshed region. The thicknesses were discretised by two partitions in each ply and ten partitions in the foam core. The projectile was simulated as a spherical analytical surface. The boundary conditions were set to be true to the real conditions. Thus, the projectile was able to move only in the through-the-thickness direction. As will be shown in the results section, the boundary conditions do not affect the residual velocity since the waves do not reach the borders of the sandwich. Nevertheless, the borders of the foam and skins were clamped to be consistent with the experimental tests, where a testing frame was used to fix the specimens. It means that all the DOFs on the side faces were restrained as illustrated in Fig. 2(c). The frictional behaviour between bodies was simulated by an exponential decay friction model instead of the classic Coulomb mode [37]. Both the elements of the plies and of the foam were deleted if any of the damage variables associated with the failure criteria reached unit value.

3. Theoretical model

In this section, a brief summary of the analytical model used to describe the energy-absorption mechanisms taking place in sandwich composite structures subjected to high-velocity impacts is presented. The following is not intended to provide a full explanation of the model but to qualitatively describe the key points of the stages and the energy-absorption mechanisms involved [38], with special focus on the first and last stages due to their importance for the ballistic limit. The structures discussed here are made by assembling a crushable PVC foam core and two composite sandwich skins consisting of woven E-glass/polyester laminates. In the first subsection, the main hypotheses are stated, and the main energy-absorption mechanisms involved in each stage are described in the second subsection.

3.1. Hypotheses of the model

The model assumes the following hypotheses:

- Although the front laminate is not very thick, the extra resistance provided by the core and the back laminate prevents the first sandwich skin from bending. This assumption allows the first sandwich skin to be considered a thick laminate according to the model proposed by [49].
- In contrast, the back composite plate is considered to behave as a thin laminate, in which membrane behaviour can be noted [39]. For this reason, the relevant variable is the relative displacement of the projectile from the first impacted facesheet of the back laminate.
- The foam is considered to be isotropic, with three different regions modelled in the constitutive law. A linear elastic behaviour between stress and strain is established up to the yield stress, followed by a perfect plastic evolution and lastly a densification process.
- The different wave movements are characterised by means of wave theory [33] and their phase velocities.

3.2. Stages of the model

The model is split into six different stages that take place sequentially. This means that the outputs of each stage are the inputs of the following one. The first stage is formulated in terms of the total instantaneous energy, which has to be equal to the current kinetic energy of the impactor added to the energy absorbed in both the laminate and the foam according to the hypothesis based on the thick woven laminates theory formulated by [49]. The sum of these two contributions must be equal to the initial kinetic energy of the projectile. The derivation with respect to the time, t, of the previous equality allows the acceleration

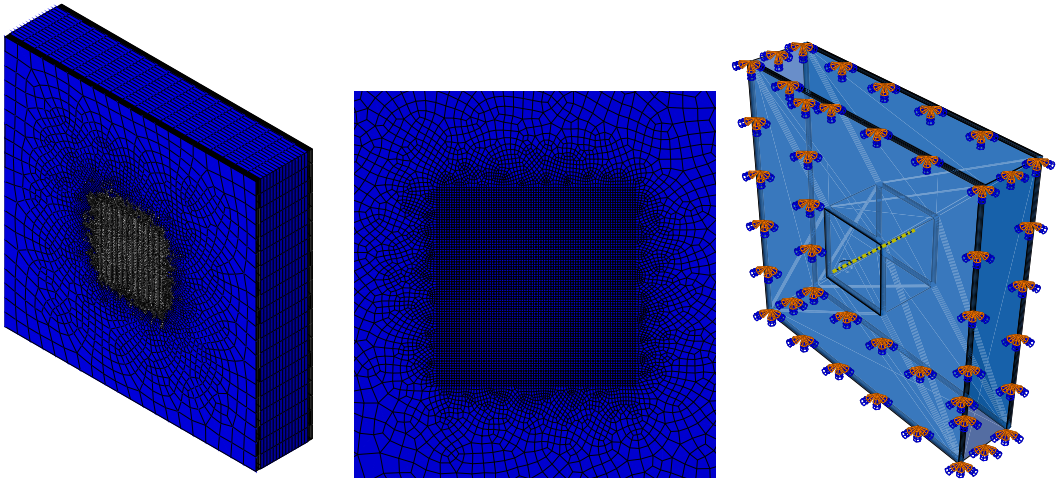

(a) Overall view (b) Detail of the central region (c) Boundary conditions

Fig. 2. Finite element discretisation and boundary conditions of the sandwich structure.

of the projectile, $a(t)$, to be obtained as a non-linear second-order differential equation which governs the first stage:

$$a(t) = \begin{cases} \frac{g(t,x(t),v(t))-h(t,v(t))v(t)-f(t,x(t))-p(t)-\frac{\pi}{24}\rho_l C_{V_{x_l}}[2v(t)^3\phi(x)\frac{d\phi}{dx}t+v(t)^2\phi(x)^2]}{m_p v(t)+\frac{\pi}{12}\rho_l C_{V_{x_l}} v(t)\phi(\bar{x})^2 t} & \text{if } t \le \frac{e_t}{C_{V_{x_l}}} \\ \frac{g(t,x(t),v(t))-h(t,v(t))v(t)-f(t,x(t))-p(t)-\frac{\pi}{12}\rho_l e_t v(t)^3\phi(x)\frac{d\phi}{dx}}{m_p v(t)+\frac{\pi}{12}\rho_l e_t v(t)\phi(\bar{x})^2} & \text{if } t > \frac{e_t}{C_{V_{x_l}}}, \end{cases} \tag{9}$$

where $C_{V_{x_l}}$ is the velocity of the through-thickness wave, e_t is the laminate thickness, ρ_l is the laminate density, $v(t)$ is the projectile velocity, $\phi(x)$ is the projected diameter of the projectile, and m_p is the projectile mass. The initial conditions for the two equations, which refer to the instant $t = 0$ when the impact takes place in the front laminate, are:

$$\begin{aligned} x(0) &= 0 \\ v(0) &= V_i, \end{aligned} \tag{10}$$

where V_i is the impact velocity of the projectile. The mathematical expressions $g(t, x(t), v(t))$, $h(t, v(t))$, $f(t, x(t))$, $p(t)$ are auxiliary functions which imply different derivatives of the energy-absorption mechanisms [38]. When the position of the projectile implies a deformation of the laminate equal to the out-of-plane compressive failure strain of the material, the first stage ends. A composite plug is pulled up and starts travelling along with the projectile. In the second stage, a perfect inelastic shock is assumed between the plug of material, with a certain linear momentum, p_{1l}, and the projectile, before and after the composite failure at the end of the first stage. Following this, in the third stage only two energy-absorption mechanisms are considered in the foam; namely, compression and shear plugging. Depending on the time spent by the waves in travelling along the laminate and foam thickness, different volumes can be delineated in order to determine the volume affected by compression. Next, in the fourth stage, the only energy-absorption mechanism considered is the energy below the foam stress-strain curve in the densification region. At the end of the densification process, a foam plug is pulled up from the foam core when the maximum strain of densification is reached. Subsequently, in the fifth stage, an instantaneous linear momentum balance between the plug of the first laminate, the foam, and the projectile is established. Following this balance, a new body formed by the projectile and the laminate and foam core plugs travels during the sixth stage.

In the sixth stage, the initial energy of the body formed by the projectile and the two plugs must be equal to the sum of the instantaneous kinetic energy of the body added to the energy absorbed up to this moment by all the energy-absorption mechanisms according to the thin woven laminates theory hypotheses formulated by [39]. The second-order differential equations that govern the stage and its initial conditions are:

$$\begin{aligned} a(t) = & \frac{g(t,x(t),v(t)) - h(t,v(t))v(t)}{(m_p + m_l + m_f)v(t) + \pi e_t \rho_l C_{V_{t_l}}{}^2[t^2 k(t,v(t))^2 v(t) + \frac{cD^{1/6}}{V_{i6}{}^2}\left(\frac{C_{V_{t_l}}}{e_t}\right)^{1/2} t^{5/2} k(t,v(t))v(t)^3]} - \\ & \frac{\pi e_t \rho_l C_{V_{t_l}}{}^2[tk(t,v(t))^2 v(t)^2 + \frac{cD^{1/6}}{V_{i6}{}^2}\left(\frac{C_{V_{t_l}}}{e_t}\right)^{1/2} t^{3/2} k(t,v(t))v(t)^4]}{(m_p + m_l + m_f)v(t) + \pi e_t \rho_l C_{V_{t_l}}{}^2[t^2 k(t,v(t))^2 v(t) + \frac{cD^{1/6}}{V_{i6}{}^2}\left(\frac{C_{V_{t_l}}}{e_t}\right)^{1/2} t^{5/2} k(t,v(t))v(t)^3]} \\ & x(0) = 0 \\ & v(0) = V_{i6}, \end{aligned} \tag{11}$$

where $C_{V_{t_l}}$ is the velocity of the transverse wave, c is a phenomenological constant, D is the flexural rigidity of the plate, m_l and m_f are the laminate and foam plug masses respectively, and $k(t, v(t))$ is a phenomenological function to account for the relative displacement [38, 39]. The expressions $g(t, x(t), v(t))$, $h(t, v(t))$ are auxiliary functions, different from the functions defined in the first stage, which again imply different derivatives of the energy-absorption mechanisms [38]. Lastly, the initial velocity of the body is V_{i6}. This stage finishes when the relative displacement between the plug and the laminate equals the laminate thickness. At that precise moment, the residual velocity is reached.

4. Results

Given that the main objective of this study is to find the suitable configuration of laminae to improve the ballistic limit of sandwich structures made of a crushable foam core and GFRP plates, the validation process is divided into two steps. In the first subsection, the FE model is validated. To this end, the FE model predictions of the ballistic response in the region of the ballistic limit are compared to experimental data and the previously validated theoretical model [38]. The relationship between the radius of the damaged area in the front and rear faces and the impact velocity is compared with the experimental results. In the second subsection, different configurations of laminae are studied to explore their influence on the ballistic limit. The energy absorption by the different mechanisms is analysed. First, the energies absorbed in the front and rear faces are compared. Secondly, the in-plane and out-of-plane energy-absorption mechanisms are assessed separately in order to provide a better understanding of the process.

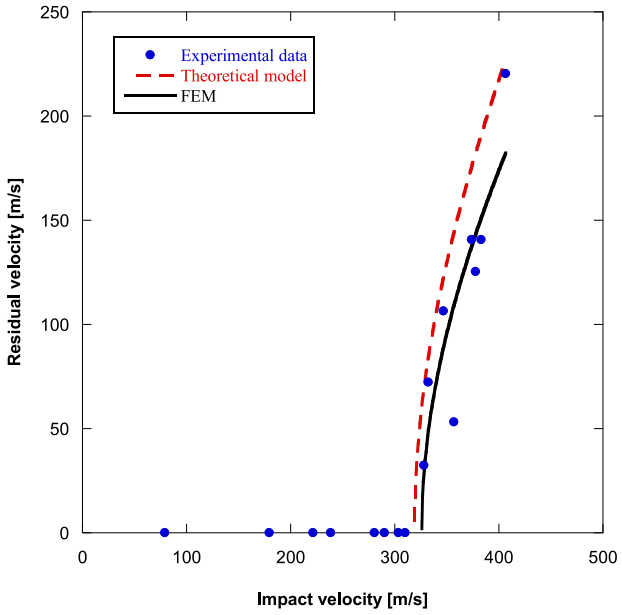

Fig. 3. Impact velocity versus residual velocity: comparison between theoretical and finite element predictions and experimental results [51].

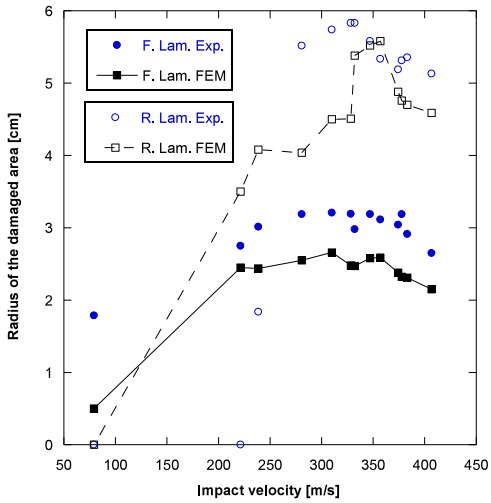

Fig. 4. Comparison between experimentally measured [17] and numerically predicted radius of the damaged area on the front and rear laminates versus impact velocity.

In the last subsection, the damaged areas obtained from the FE model are compared to the surfaces affected by the projectile impact in the experiment.

4.1. Validation of the finite element model

The validation study is focused on the ballistic limit of the sandwich structure. In the experimental tests carried out by [51], a Sabre Ballistics model A1G gas gun was used. Impact velocity was controlled by regulating the pressure in the system and either of two gases were employed, helium or argon. Spherical steel projectiles of 7.5 mm diameter and 1.7 g mass were used. A Photron FASTCAM-ultima APX high-speed video camera was used to record the impact tests. The data acquisition system of the camera was adjusted to gather information in a window of 50,000 frames per second. It took 16 experimental result tests, because the interesting zone in this study is close to the ballistic limit, which was measured to be 343 m/s. In these tests, the ballistic limit is experimentally defined as the impact velocity required to perforate the target 50% of the time. This statistical definition makes sense for experiments. For the analytical and numerical models, each impact velocity has one residual velocity associated with it. Therefore, the ballistic limit is simply taken as the first impact velocity with a non-zero residual velocity. As explained in a previous section, the configuration of laminae is denoted by two numbers; the number of plies on the front and rear faces respectively. Since the configuration of laminae will vary, and the original ballistic limit for the neutral configuration, 5-5, is 343 m/s, a reasonable prediction is that the configuration presenting the highest ballistic limit is bounded below 400 m/s, which would be a ballistic limit improvement of more than 15%. For this reason, the finite element model is only validated within this range of velocities. A set of 16 FEM simulations were conducted to reproduce the available experimental tests. Since the theoretical model is less computationally expensive, simulations were performed for each initial velocity. The comparison between the theoretical and finite element predictions of the residual velocity versus the impact velocity with the experimental data available [51] is presented in Fig. 3.

Fig. 3 shows good agreement between both the theoretical and finite element models and the experimental data. The ballistic limit found experimentally through a Lambert-Jonas adjustment is 343 m/s while those predicted by the theoretical and finite element models are 322 m/s and 326 m/s respectively. Therefore, the finite element model captures the value of the ballistic limit for the reference configuration (5-5) reasonably well (error below 10%). Moreover, the fit of the curves in the region of the ballistic limit is fairly good. The theoretical model slightly overestimates the residual velocities given by the experimental data but the finite element model predictions are very accurate near the ballistic limit. To complete the validation, the damaged area from the experiment was measured from photographs of the impacted specimens using free digital image-processing software; this was possible because the material of the skins was translucent [17]. Fig. 4 shows that the damaged areas predicted by the FE model on the front and rear laminates follow the same trends when compared with the experiments, revealing a peak for impact velocities near the ballistic limit. This peak is softer for the front laminates.

It can be observed that in both cases the size of the damaged area becomes larger as impact velocities approximate the ballistic limit where the contact time, and thus the transverse wave and delamination are at a maximum. Consequently, both models are suitable for use in the search for a configuration of laminae to improve the ballistic limit with a given number of plies.

4.2. Study of ballistic limit sensitivity with respect to configuration and energy absorption

The main objective of this section is to determine the most appropriate configuration of plies or at least to discover useful trends to establish the ballistic limit. Since the original sandwich skins of the sandwich structure were made of 0.6 mm thick plies (each sandwich skin consists of 5 assembled plies), the configurations proposed are all the possible distributions of plies with the same total thickness for the two sandwich skins. To this end, a set of finite element and theoretical simulations were considered with all possible configurations of laminae. For each configuration, different simulations of impact tests were performed numerically and analytically for different projectile impact velocities to determine the predicted ballistic limit. In the FE model, for each configuration, a simulation was performed every 10 m/s. When the residual velocity changed from zero to non-zero in two consecutive simulations, the ballistic limit was set as the mean of the impact velocities of the two simulations. In the theoretical model, for each configuration, a simulation was carried out every 1 m/s. The ballistic limit was taken as the first impact velocity value with a non-zero residual velocity. The only parameter changed from one

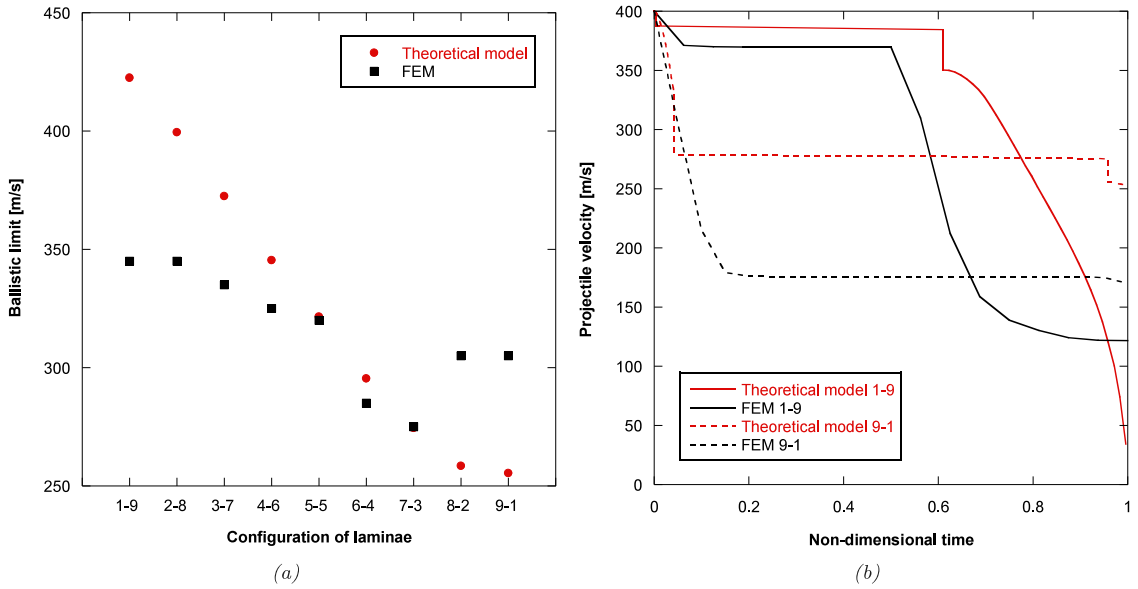

Fig. 5. (a) Ballistic limit versus laminate configuration ([number of laminae on front face]-[number of laminae on rear face]). (b) Projectile velocity versus non-dimensional time for an impact velocity of 400 m/s, comparison between theoretical and FE predictions for configurations 1-9 and 9-1.

configuration to another, apart from the impact velocities to look for the ballistic limit, was the number of plies constituting the front and rear skins. The results of this analysis are shown in Fig. 5(a).

Fig. 5(a) shows that the configuration where the ballistic limit is the highest is reached with the 1-9 configuration. This prediction is consistent between the theoretical and finite element models. Furthermore, both models agree in describing the same descending trend in the ballistic limit when the number of plies on the front face skin is increased while the number in the rear face is reduced.

Even though the trends are the same, there are notable differences between the ballistic predictions of the two models in the range sufficiently different from the neutral configuration (5-5), where the predictions are almost equal. All the energy-absorption mechanisms described in the theoretical model are accounted for in the FE model by means of the various failure criteria. Therefore, it can be inferred that the differences observed in Fig. 5(a) are mainly associated with the moment transfers considered in the theoretical model and to differences in the failure criteria. On the one hand, these inelastic shocks are indeed one of the most effective mechanisms to decrease projectile velocity in the analytical model [38] as shown in Fig. 5(b). In this model, the plug of material formed in the first stage is smaller, as there are few plies on the front face to influence the linear momentum of the plug, p_{1l}. This effect produces a lower projectile velocity and therefore a higher ballistic limit in configurations with fewer plies in the first sandwich skin (4-6 to 1-9) than the neutral configuration. As the number of plies is progressively higher, the sandwich skins' capacity to decrease the projectile velocity is affected. This causes the theoretical predictions of the ballistic limit to decrease significantly faster than the FE predictions. Additionally, no moment transfer between the projectile and the plugs occurs in the FE approach. When an element is deleted to avoid distortion problems, the corresponding pivot in the mass matrix becomes null. Therefore, there is a continuum loss of laminate mass during the process, since it is impossible to reproduce the moment transfers assumed in the theoretical model. Since this effect is not accounted for in the FE model, the decrease in the ballistic limit as more plies are added to the front face is smoother than in the theoretical model. Fig. 5(b) shows that if the loss of velocity in the inelastic shocks were added to the numerical model, the prediction of residual velocities would be almost identical in the two models for the 1-9 configuration. Furthermore, it must be kept in mind that the two models are subject to different hypotheses. For instance, the analytical model uses failure criteria based on maximum strain, while the deletion of elements is decided by means of a continuum damage model in the FE model. Even though the failure criteria are formulated with equivalences, it is unavoidable that certain differences arise. Fig. 5(b) illustrates this idea for the 9-1 configuration. In the analytical model, the laminate absorbs energy only until the criterion of maximum deformation is met before the projectile has travelled through all the laminate in the first stage. In contrast, the FE model allows the elements to absorb energy through the entire projectile path, which explains why the loss of energy is higher than in the analytical model in early stages and thus explains the differences in Fig. 5(b) for the 9-1 configuration. This set of results indicates that the ballistic limit and hence the projectile contact time depend not only on the density of the core [57] or sandwich thickness [58] but also on the configuration of the plies when the rest of the parameters remain constant.

Another important feature that helps to better understand the trend of the ballistic limit shown in Fig. 5(a) is the energy absorbed by the front and rear faces. The non-dimensional energy absorbed by the front and rear faces predicted by the two models are compared for the different configurations of laminae in Fig. 6. Fig. 6(a) shows this comparison for an 8-2 configuration of the laminae and Fig. 6(b) presents the comparison for all analysed configurations for a projectile impact velocity of 400 m/s.

The first aspect to highlight in Fig. 6(b) is the near-total lack of energy absorption by the front face in the 1-9 configuration in the theoretical model prediction. After this first configuration, the energy absorbed by the front face skin increases as more laminae are added to this face while the energy absorbed by the rear face skin decreases. This trend is followed in both models and it is consistent with expectations. Both models predict that the front face absorbs almost all the energy in the 9-1 configuration. At a certain intermediate configuration, there is a point where the energy absorbed by the front and rear face skins is equal. Note that for the 4-6 configuration the FE model predicts greater energy absorption by the front face skin although the rear face skin has two more plies. Symmetrically, for the 6-4 configuration, the theoretical model predicts greater energy absorption by the rear face skin even though the front face skin has two more plies. Therefore, more plies do not necessarily produce greater energy absorption. Although the energy absorbed by the front and rear skins cannot be experimentally determined, by comparing the energy values provided by the models, Fig. 5(a) can suggest which model predicts this result more accurately.

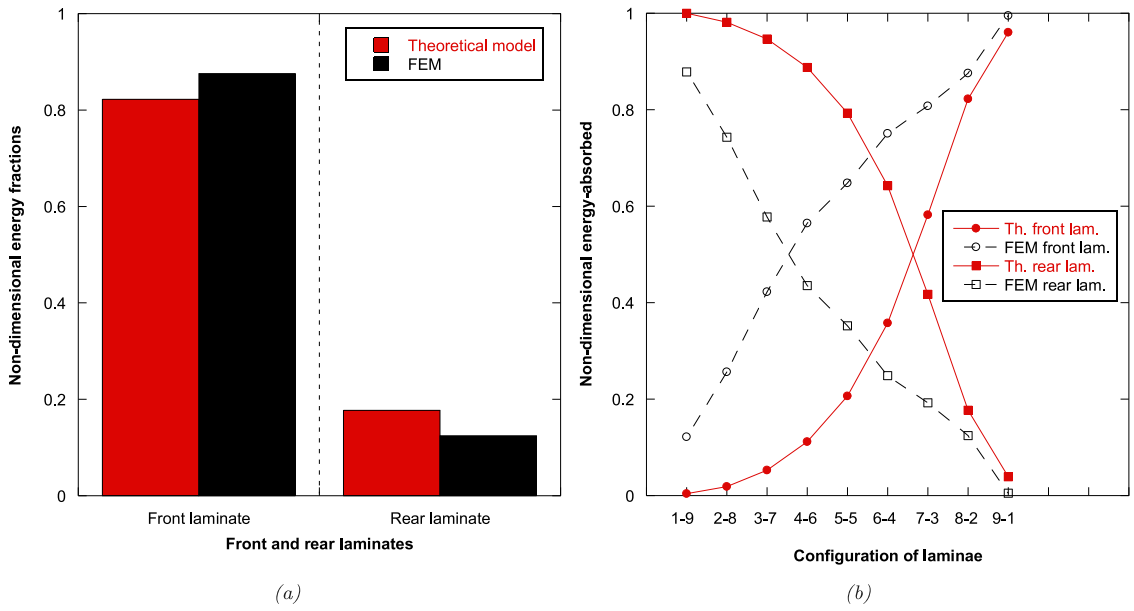

Fig. 6. Comparison of the non-dimensional energy fraction predictions of the front and rear faces between the theoretical and finite element models for: (a) an 8-2 configuration of the laminae; (b) all configurations of laminae at a 400 m/s projectile impact velocity.

Since the ballistic limit grows with the number of plies on the rear sandwich skin, it is reasonable to think that the rear sandwich skin absorbs more energy. Therefore, the theoretical model predicts that the energy absorbed by the rear skin is larger for more configurations than the FEM as shown in Fig. 6(b) (from 1-9 to 6-4 even though there are more plies on the front skin in the latter configuration). Thus it is reasonable to conclude that the predictions given by the theoretical model are more accurate in this regard.

Lastly, the distribution of the energy absorbed in in-plane (I-P) and out-of-plane (O-O-P) energy-absorption mechanisms for the different configurations can give some insights about the failure modes and thus the ballistic responses of these sandwich structures. The in-plane energy-absorption mechanisms considered in the theoretical model are elastic deformation of fibres (Eqs. (2), (3) in the FE model), tensile failure of fibres (Eqs. (2), (3) in the FE model), and delamination and matrix cracking (Eq. (4) in the FE model). The out-of-plane mechanisms are compression (Eq. (6) in the FE model), shear plugging (Eq. (5) in the FE model) and laminate acceleration (kinetic energy of the elements in the FE model) throughout the impact direction. Fig. 7(a) shows this comparison for an 8-2 configuration of laminae and Fig. 7(b) presents the comparison for all the possible configurations analysed, again for a projectile impact velocity of 400 m/s.

Fig. 7 shows the dominant role of the O-O-P energy-absorption mechanisms that govern the penetration process in all the configurations studied. Note that the relative importance of O-O-P and I-P mechanisms remains practically constant in the theoretical model predictions and tends to stabilise in the FE model, the results being close to constant within most of the range studied (from 2-8 to 9-1). Overall, it can be stated that both models' predictions are in agreement in terms of the relative importance and constant trend of the I-P/O-O-P mechanisms for all the laminae configurations.

4.3. Experimental and numerical damaged area

As the FE model is formulated to take into account the different failure modes, it is essential to assess whether it can qualitatively and quantitatively predict the morphology of the damaged area. To this end, the experimental damaged areas in the front and rear faces of the sandwich structure are compared to the numerically obtained damaged surfaces for the impact velocities analysed in this paper. The comparison is carried out for the neutral configuration, for which experimental data is available. The results are presented as a function of the radius instead of the size of the area as all the damaged surfaces turn out to be circular. The damaged area on the front laminate is similar in shape and size in all the specimens. The FE model accurately predicts the damaged area both qualitatively and quantitatively, as can be seen in Fig. 9. As already stated, the affected areas are circular with a size similar to the diameter of the projectile. From this result, it can be inferred that local phenomena such as compression and shear plugging are responsible for the failure of the front laminate, because these failure modes provoke local damage [37]. In Fig. 8, the Cauchy stress (σ_{22}) on both laminates is shown for a sandwich structure impacted at 310 m/s. The small size of the affected area on the front laminate compared to the rear laminate supports the hypothesis that the front laminate fails due to the local failure modes mentioned above.

As already noted, the damaged area on the rear laminate is clearly larger than that on the front laminate. This agrees with the findings reported by [37,59,60]. Due to the boundary conditions of the experiments, the rear laminate has a membrane-like behaviour allowing the fibres to withstand large deformations before breaking. The out-of-plane acceleration of the laminate contributes to reducing the projectile velocity mainly by means of fibre failure and elastic deformation of fibres [38]. This out-of-plane movement leads to larger delaminations compared to the front laminate. Illustrating the failure modes, Fig. 8(b) shows the fibre failure in a sandwich structure impacted at 310 m/s, in which breakage of the four main fibres can be noticed. This shows that σ_{22} responsible for this failure is greater on the rear laminate as shown in the comparison between Figs. 8(a) and 8(b) for the reason explained above. Lastly, to visually back up the results shown in Fig. 4, the experimentally obtained and numerical predicted damaged areas for velocities below, around and above the ballistic limit are shown in Fig. 9, showing that the general trend of the experimental and numerical results in terms of the size of the damaged surface is similar. Rear laminates are shown in Fig. 9 since the damaged area is larger and thus it can be better visualised. Overall, the predictive capability of the FE model in terms of representing the damaged area is proven according to the shapes and qualitative trends experimentally shown.

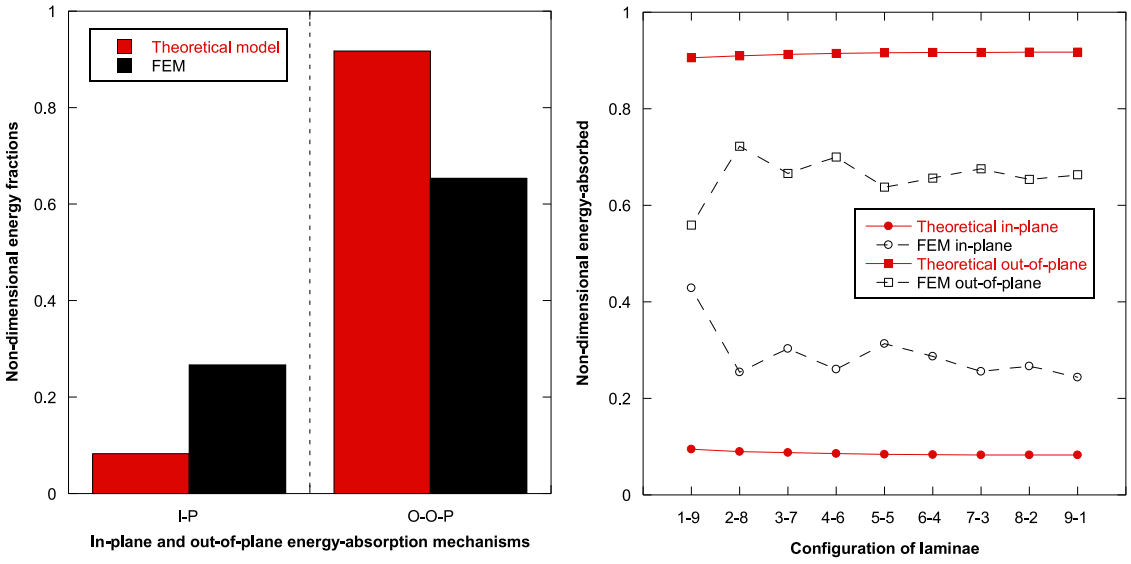

Fig. 7. Comparison of non-dimensional energy fraction predictions of in-plane (I-P) and out-of-plane (O-O-P) energy-absorption mechanisms between the theoretical and finite element models for (a) an 8-2 configuration of laminae; (b) all configurations of laminae at a 400 m/s projectile velocity.

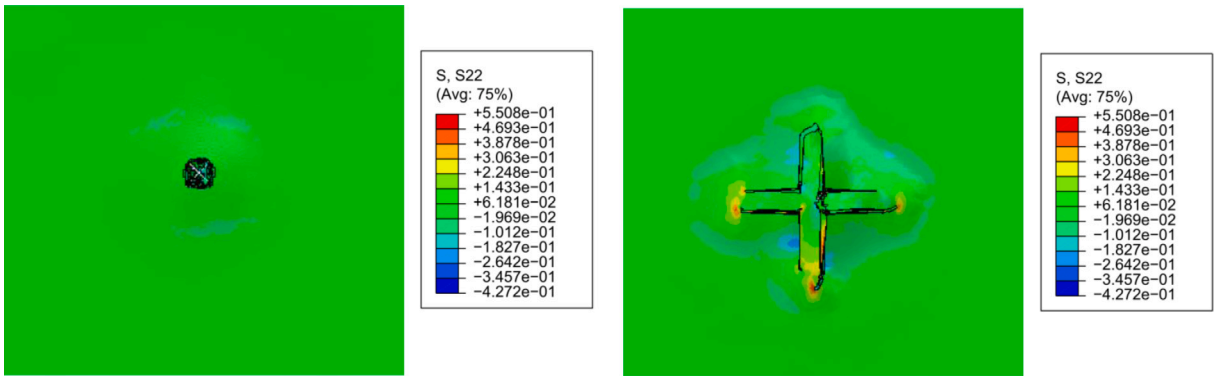

Fig. 8. Representation of Cauchy stress (σ_{22}) on front and back laminates of a sandwich structure impacted at 310 m/s at 0.3 ms.

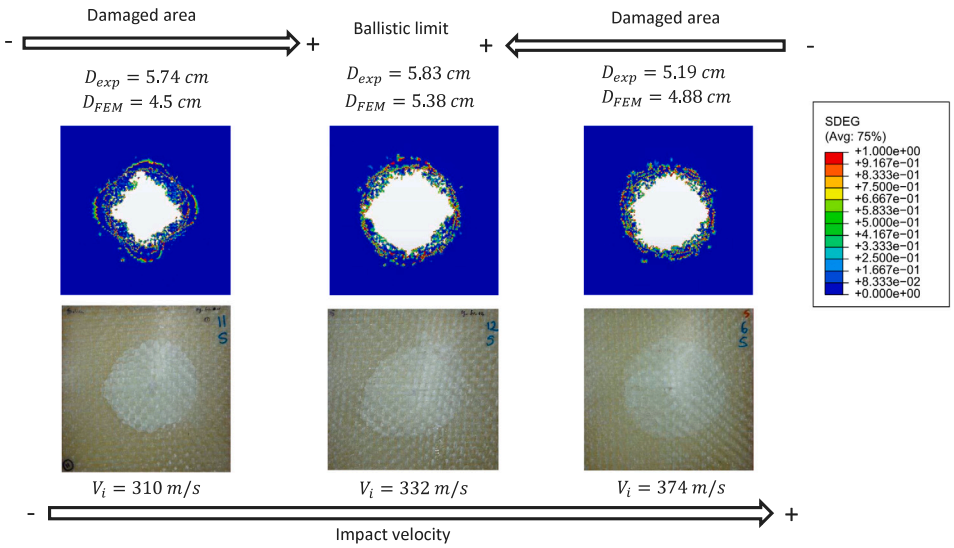

Fig. 9. Comparison of numerically and experimentally predicted damaged areas on the rear laminates at increasing impact velocities.

5. Conclusions

In this work, a sensitivity study was carried out to determine the most suitable configuration in composite structures subjected to high-velocity impacts. The typology of the structure studied was a sandwich made of two GFRP sandwich skins with a crushable foam core between them. Two models, analytical and numerical, were used to analyse the perforation process and they were able to accurately predict the ballistic limit after being validated with experimental data. Different configurations were studied in which the numbers of plies on the front and rear faces were varied, keeping the total number constant. All the analyses were performed for a projectile impact velocity of 400 m/s and the energy absorbed for each configuration was assessed. Lastly, the energy absorbed in each configuration by the different in-plane and out-of-plane energy-absorption mechanisms was also analysed using both theoretical and numerical approaches. The conclusions that can be drawn from this study can be summarised as follows:

- For a sandwich structure of a given thickness, the distribution of plies between the front and rear faces has to be taken into account in addition to the areal density in order to determine the ballistic limit or the energy absorbed by each energy-absorption mechanism.
- The ballistic limit predictions obtained from both models were the same in the neutral configuration. Although the descending trend (as the number of plies on the rear face was decreased) was well-captured through both approaches, there were quantitative differences between them. Whilst the theoretical approach took into account inelastic shocks in the plug formation processes and hence predicted a steeper descent, the FE model described a smoother evolution for the ballistic limit. Regardless of these differences, both models were proved to be appropriate to analyse the behaviour of the ballistic limit. In view of the results obtained, the configuration providing the highest ballistic limit was 1-9, meaning that the most accurate strategy to improve the ballistic limit consists of concentrating the composite material in the rear face, in which bending effects are dominant.
- In relative terms, the energy absorbed by the front face went from practically zero to the whole of the energy as the sandwich skin configuration was changed from 1-9 to 9-1. The fraction of the energy absorbed by the rear face was almost whole when the configuration was 1-9, decreasing to practically zero in the 9-1 configuration. Again, there were numerical differences in the energy absorbed by the front and rear faces, obtaining identical qualitative behaviours from both approaches. As already noted, there were intermediate configurations in which the sandwich skin that absorbed larger energy fractions was the face with fewer layers. These enlightening results allow us to state that ballistic performance in sandwich structures depends not only on the amount of material included but also on finding the most suitable place for it. Lastly, the configuration in which both sides of the laminate absorbed equal energy fractions was determined. While this configuration is estimated to be within the 7-3 to 6-4 range by the theoretical approach, it happened to be located in the 3-7 to 4-6 range according to the FE model.
- Out-of-plane energy-absorption mechanisms play a more important role than in-plane mechanisms. The fractions predicted by both approaches for both groups of mechanisms tended to be approximately constant for all laminae configurations.
- The circular shaped damaged area of the specimens tested is accurately predicted by the FE model. The area of the damaged surface is larger in the rear laminates due to the out-of-plane movement. A peak in the area of the damaged areas is experimentally and numerically observed when the impact velocities approach the ballistic limit, leading to the conclusion that main trends are well captured by the FE model.

CRediT authorship contribution statement

L. Alonso: Conceptualization, Methodology, Software, Investigation, Writing - original draft, Writing - review & editing, Visualization. **A. Solis:** Conceptualization, Methodology, Software, Investigation, Writing - original draft, Writing - review & editing, Visualization. **S.K. García-Castillo:** Conceptualization, Writing - review & editing, Funding acquisition.

Declaration of competing interest

The authors declare that they have no known competing financial interests or personal relationships that could have appeared to influence the work reported in this paper.

Data availability

Data will be made available on request.

References

[1] Guangyong S, Tong S, Chen D, Gong Z, Li Q. Mechanical properties of hybrid composites reinforced by carbon and basalt fibers. Int J Mech Sci 2018;148:636–51. http://dx.doi.org/10.1016/j.ijmecsci.2018.08.007.
[2] Dhari R, Patel N, Wang H, Hazell P. Progressive damage modeling and optimization of fibrous composites under ballistic impact loading. Mech Adv Mater Struct 2019;1–18. http://dx.doi.org/10.1080/15376494.2019.1655688.
[3] Maimí P, Camanho P, Mayugo J, Dávila C. A continuum damage model for composite laminates: Part II-computational implementation and validation. Mech Mater 2007;39:909–19. http://dx.doi.org/10.1016/j.mechmat.2007.03.006.
[4] Hajikazemi M, Van Paepegem W. A variational model for free-edge interlaminar stress analysis in general symmetric and thin-ply composite laminates. Compos Struct 2018;184:443–51. http://dx.doi.org/10.1016/j.compstruct.2017.10.012.
[5] Hu F, Soutis C, Edge E. Interlaminar stresses in composite laminates with a circular hole. Compos Struct 1997;(37):223–32. http://dx.doi.org/10.1016/S0263-8223(97)80014-1.
[6] Su Z, Tay T, Ridha M, Chen B. Progressive damage modeling of open-hole composite laminates under compression. Compos Struct 2015;122:507–17. http://dx.doi.org/10.1016/j.compstruct.2014.12.022.
[7] Soutis C, Curtis P, Fleck N. Static compression failure of notched carbon fibre composite. Proceed: Mathemat Phys Sci 1993;(440):241–56. http://dx.doi.org/10.1177/002199839002400505.
[8] AhmadvashAghbash S, Breite C, Mehdikhani M, Swolfs Y. Longitudinal debonding in unidirectional fibre-reinforced composites: Numerical analysis of the effect of interfacial properties. Compos Sci Technol 2022;(218):109117. http://dx.doi.org/10.1016/j.compscitech.2021.109117.
[9] Heide-Jørgensen S, Budzik M, Ibsen C. Three-dimensional, multiscale homogenization for hybrid woven composites with fiber-matrix debonding. Compos Sci Technol 2022;(218):109204. http://dx.doi.org/10.1016/j.compscitech.2021.109204.
[10] Solis A, Barbero-Pozuelo E, Sánchez-Sáez. Analysis of the influence of ply-orientation in delamination progression in composites laminates using the Serial/Parallel Mixing Theory. Compos Sci Technol 2021;(211). http://dx.doi.org/10.1016/j.compscitech.2021.108847.
[11] Lei H, Yao K, Wen W, Zhou H, Fang D. Experimental and numerical investigation on the crushing behavior of sandwich composite under edgewise compression loading. Composites B 2016;94(1):34–44. http://dx.doi.org/10.1016/j.compositesb.2016.03.049.
[12] Zhang X, Liu T, He N, Jia G. Investigation of two finite element modelling approaches for ballistic impact response of composite laminates. Int J Crashrothiness 2016;22(4):377–93. http://dx.doi.org/10.1080/13588265.2016.1270495.
[13] Hazzard M, Trask R, Heisserer U, Van Der Kamp M, Hallett S. Finite element modelling of Dyneema® composites: From quasi-static rates to ballistic impact. Composites A 2018;115:31–45. http://dx.doi.org/10.1016/j.compositesa.2018.09.005.
[14] Zhu G, Sun G, Yu H, Li S, Li Q. Energy absorption of metal, composite and metal/composite hybrid structures under oblique crushing loading. Int J Mech Sci 2018;135:458–83. http://dx.doi.org/10.1016/j.ijmecsci.2017.11.017.
[15] Nurazzi N, Asyraf M, Khalina A, Abdullah N, Aisyah H, Ayu Rafiqah S, et al. A review on natural fiber reinforced polymer composite for bullet proof and ballistic applications. Polymers 2021;(646). http://dx.doi.org/10.3390/polym13040646.
[16] Atas C, Potoglu U. The effect of face-sheet thickness on low-velocity impact response of sandwich composites with foam cores. J Sandw Struct Mater 2016;18(2):215–28. http://dx.doi.org/10.1177/1099636215613775.

[17] García-Castillo S, Buitrago B, Barbero E. Behavior of sandwich structures and spaced plates subjected to high-velocity impacts. Polym Compos 2011;32(2):290–6. http://dx.doi.org/10.1002/pc.21047.
[18] Elnasri I, Zhao H. Impact perforation of sandwich panels with aluminum foam core: A numerical and analytical study. Int J Impact Eng 2016;(96):50–60. http://dx.doi.org/10.1016/j.ijimpeng.2016.05.013.
[19] Cui T, Zhang J, Li K, Peng J, Chen H, Qin Q, et al. Ballistic limit of sandwich plates with a metal foam core. J Appl Mech Trans ASME 2022;89:021006. http://dx.doi.org/10.1115/1.4052835.
[20] Usta F, Turkmen HS, Scarpa F. High-velocity impact resistance of doubly curved sandwich panels with re-entrant honeycomb and foam core. Int J Impact Eng 2022;165:104230. http://dx.doi.org/10.1016/j.ijimpeng.2022.104230.
[21] Ryan S, Schaefer F, Destefanis R, Lambert M. A ballistic limit equation for hypervelocity impacts on composite honeycomb sandwich panel satellite structures. Adv Space Res 2008;(41):1152–66. http://dx.doi.org/10.1016/j.asr.2007.02.032.
[22] Avachat S, Zhou M. Effect of facesheet thickness on dynamic response of composite sandwich plates to underwater impulsive loading. Exp Mech 2012;(52):83–93. http://dx.doi.org/10.1007/s11340-011-9538-4.
[23] Avachat S, Zhou M. Effect of core density on deformation and failure in sandwich composites subjected to underwater impulsive loads. Int J Multiphys 2012;6(3):241–65. http://dx.doi.org/10.1260/1750-9548.6.3.241.
[24] Rahimijonoush A, Bayat M. Experimental and numerical studies on the ballistic impact response of titanium sandwich panels with different facesheets thickness ratios. Thin-Walled Struct 2020;(157):107079. http://dx.doi.org/10.1016/j.tws.2020.107079.
[25] Hegde S, Hojjati M. Effect of core and facesheet thickness on mechanical property of composite sandwich structures subjected to thermal fatigue. Int J Fatigue 2019;(127):16–24. http://dx.doi.org/10.1016/j.ijfatigue.2019.05.031.
[26] Sun G, Chena D, Wang H, Hazellc P, Lib Q. High-velocity impact behaviour of aluminium honeycomb sandwich panels with different structural configurations. Int J Impact Eng 2018;(122):119–36. http://dx.doi.org/10.1016/j.ijimpeng.2018.08.007.
[27] Ibrahim M. Nondestructive evaluation of thick-section composites and sandwich structures: A review. Composites A 2014;(64):36–48. http://dx.doi.org/10.1016/j.compositesa.2014.04.010.
[28] Jover N, Shafiq B, Vaidya U. Ballistic impact analysis of balsa core sandwich composites. Composites B 2014;(67):160–9. http://dx.doi.org/10.1016/j.compositesb.2014.07.002.
[29] Naik N, Doshi A. Ballistic impact behaviour of thick composites: Analytical formulation. AIAA J 2005;43(7):1525–36. http://dx.doi.org/10.2514/1.11993.
[30] Naik N, Doshi A. Ballistic impact behaviour of thick composites:Parametric studies. Compos Struct 2008;82(3):447–64. http://dx.doi.org/10.1016/j.compstruct.2007.01.025.
[31] Alonso L, Navarro C, García-Castillo S. Analytical models for the perforation of thick and thin thicknesses woven-laminates subjected to high-velocity impact. Composites B 2018;143(15):292–300. http://dx.doi.org/10.1016/j.compositesb.2018.01.030.
[32] Hoo Fatt M, Park K. Perforation of honeycomb sandwich plates by projectiles. Composites A 2000;(31):889–99. http://dx.doi.org/10.1016/S1359-835X(00)00021-X.
[33] Smith J, F.L. M, Schiefer H. Stress-strain relationships in yarns subjected to rapid impact loading: Part V: Wave propagation in long textile yarns impacted transversally. J Res Natl Bureau Standards 1958;60(5):517–34. http://dx.doi.org/10.1177/004051755802800402.
[34] Hoo Fatt M, Sirivolu D. A wave propagation model for the high velocity impact response of a composite sandwich panel. Int J Impact Eng 2009;37(14):117–30. http://dx.doi.org/10.1016/j.ijimpeng.2009.09.002.
[35] Hoo Fatt M, Park K. Dynamic models for low-velocity impact damage of composite sandwich panels – Part A: Deformation. Compos Struct 2001;52(1):335–52. http://dx.doi.org/10.1016/S1359-835X(00)00020-8.
[36] Feli S, Namdari-Pour M. An analytical model for composite sandwich panels with honeycomb core subjected to high-velocity impact. Composites B 2012;43(5):2439–47. http://dx.doi.org/10.1016/j.compositesb.2011.11.028.
[37] Alonso L, Martínez-Hergueta F, Garcia-Gonzalez D, Navarro C, García-Castillo S, Teixeira-Dias F. A finite element approach to model high-velocity impact on thin woven GFRP plates. Int J Impact Eng 2020;142. http://dx.doi.org/10.1016/j.ijimpeng.2020.103593.
[38] Alonso L, Solis A. High-velocity impact on composite sandwich structures: A theoretical model. Int J Mech Sci 2021;201:106459. http://dx.doi.org/10.1016/j.ijmecsci.2021.106459.
[39] Alonso L, Garcia-Gonzalez D, Martínez-Hergueta F, Navarro C, Teixeira-Dias F, García-Castillo S. Modeling high velocity impact on thin woven composite plates: A non-dimensional theoretical approach. Composites B 2021. http://dx.doi.org/10.1080/15376494.2021.1878402.
[40] Xiao J, Gama B, Gillespie Jr. J. Progressive damage and delamination in plain weave S-2 glass/SC-15 composites under quasi-static punch-shear loading. Compos Struct 2007;78(2):182–96. http://dx.doi.org/10.1016/j.compstruct.2005.09.001.
[41] Lopes C, Camanho P, Gürdal Z, Miamí P, González E. Low-velocity impact damage on dispersed stacking sequence laminates. Part II: Numerical simulations. Compos Sci Technol 2009;69(7–8):937–47. http://dx.doi.org/10.1016/j.compscitech.2009.02.015.
[42] Muñoz F, Martínez-Hergueta F, Gálvez F, González C, Llorca J. Ballistic performance of hybrid 3D woven composites: Experiments and simulations. Compos Struct 2015;127(1):141–51. http://dx.doi.org/10.1016/j.compstruct.2015.03.021.
[43] Martínez-Hergueta F, Ares D, Ridruejo A, Wiegand J, Petrinic N. Modelling the in-plane strain rate dependent behaviour of woven composites with special emphasis on the non-linear shear response. Compos Struct 2019;210(15):840–57. http://dx.doi.org/10.1016/j.compstruct.2018.12.002.
[44] Chang F, Chang K. A progressive damage model for laminated composites containing stress concentrations. J Compos Mater 1987;21:834–55. http://dx.doi.org/10.1177/002199838702100904.
[45] ASTM–Standard–D3410/D–3410M–95. Standard test method for compressive properties of polymer matrix composite materials with unsupported gage section by shear loading. 2010.
[46] ASTM–Standard–D732–02. Standard test method for shear strength of plastics by punch tool. 2002.
[47] Hashin Z. Failure criteria for unidirectional fiber composites. J Appl Mech 1980;47(2):329–34. http://dx.doi.org/10.1115/1.3153664.
[48] ASTM–Standard–D695–96. Standard test method for compressive properties of rigid plastics. 1995.
[49] Alonso L, Garcia-Gonzalez D, Navarro C, García-Castillo S. A non-dimensional theoretical approach to model high-velocity impact on thick woven plates. Steel Compos Struct 2021. http://dx.doi.org/10.12989/scs.2021.38.6.717.
[50] Turon A, Dávila C, Camaho P, Coste J. An engineering solution for mesh size effects in the simulation of delamination using cohesive zone models. Eng Fract Mech 2007;74(10):1665–82. http://dx.doi.org/10.1016/j.engfracmech.2006.08.025.
[51] Iváñez I, Santiuste C, Barbero E, Sánchez-Sáez. Numerical modelling of foam-cored sandwich plates under high-velocity impact. Compos Struct 2011;93:2392–9. http://dx.doi.org/10.1016/j.compstruct.2011.03.028.
[52] Smith M. ABAQUS/Standard user's manual, version 6.14. United States: Dassault Systèmes Simulia Corp; 2014.
[53] Kenane M, Benzeggagh M. Mixed-mode delamination fracture toughness of unidirectional glass/epoxy composites under fatigue loading. Compos Sci Technol 1997;57(5):597–605. http://dx.doi.org/10.1016/S0266-3538(97)00021-3.
[54] Pascuzzo A, Greco F, Leonetti L, Lonetti P, Pranno A, Ronchei C. Investigation of mesh dependency issues in the simulation of crack propagation in quasi-brittle materials by using a diffuse interface modeling approach. Fatigue Fract Eng Mater Struct 2022;45(3):801–20. http://dx.doi.org/10.1111/ffe.13635.
[55] Ren X, Guan X. Three dimensional crack propagation through mesh-based explicit representation for arbitrarily shaped cracks using the extended finite element method. Eng Fract Mech 2017;177:218–38. http://dx.doi.org/10.1016/j.engfracmech.2017.04.007.
[56] Zhou F, Molinari JF. Dynamic crack propagation with cohesive elements: A methodology to address mesh dependency. Internat J Numer Methods Engrg 2004;59(1):1–24. http://dx.doi.org/10.1002/nme.857.
[57] Tao Q, Ren P, Shi L, Zhao Z, Tang Y, Ye R, et al. Energy absorption and impact behavior of composite sandwich panels under high-velocity spherical projectile. Int J Impact Eng 2022;162:104143. http://dx.doi.org/10.1016/j.ijimpeng.2021.104143.
[58] Buitrago BL, García-Castillo S, Barbero E. Experimental analysis of perforation of glass/polyester structures subjected to high-velocity impact. Mater Lett 2010;64(6):1052–4. http://dx.doi.org/10.1016/j.matlet.2010.02.007.
[59] Alonso L, Navarro C, García-Castillo S. Experimental study of woven-laminates structures subjected to high-velocity impact. Mech Adv Mater Struct 2018. http://dx.doi.org/10.1080/15376494.2018.1526354.
[60] Gil-Alba R, Alonso L, Navarro C, García-Castillo S. Morphological study of damage evolution in woven-laminates subjected to high-velocity impact. Mech Adv Mater Struct 2019;26(24):2023–9. http://dx.doi.org/10.1080/15376494.2019.1692264.